Thin Solid Films 693 (2020) 137704

Contents lists available at ScienceDirect

Thin Solid Films

journal homepage: www.elsevier.com/locate/tsf

Thermal transport on composite thin films using graphene nanodots and polymeric binder

Siyong Gu[a], Chien-Te Hsieh[b,c,*], Wen-Ching Lin[b], Bikash Chandra Mallick[b], Yasser Ashraf Gandomi[d]

[a] Fujian Provincial Key Laboratory of Functional Materials and Applications, School of Materials Science and Engineering, Xiamen University of Technology, Xiamen 361024, China
[b] Department of Chemical Engineering and Materials Science, Yuan Ze University, Taoyuan 32003, Taiwan
[c] Department of Mechanical, Aerospace, and Biomedical Engineering, University of Tennessee, Knoxville, TN 37996, United States
[d] Department of Chemical Engineering, Massachusetts Institute of Technology, Cambridge, MA 02142, United States

ARTICLE INFO

Keywords:
Graphene nanodots
Composite thin films
Thermal conductivity
Electrical conductivity
Polymeric coating

ABSTRACT

Series of composite thin films consisted of graphene nanodots (GNDs) and water-based binder (i.e., polyvinylpyrrolidone and polyvinyl alcohol) are designed and fabricated for nano-engineering devices with enhanced thermal and electrical conductivities. A thermal pyrolysis of citric acid and urea is adopted to synthesize crystalline GNDs under IR irradiation. The as-prepared GNDs are uniformly coated over three types of substrates including Cu foil, cotton cloth and filter paper. The GND thin films emit tunable fluorescence upon thermal treatment of GNDs at 400 °C in helium atmosphere. The thermally treated GND-based thin film exhibits excellent thermal as well as electrical conductivity compared to bare GNDs and reduced graphene oxide sheets. The enhanced conductivity is due to the reduced oxidation level induced by the thermal treatment on GNDs samples which subsequently decreases the photon scattering. With increasing weight loading, GNDs can serve not only as connective point but also as stuff, offering a well-developed conductive path for the heat dissipation. Accordingly, the design of GND thin film is promising for enhanced thermal management for electronic and photonic applications since it enables engineering the fluorescence emission with substantially increased thermal and electrical conductivities.

1. Introduction

Fluorescent graphene nanodots (GNDs) are zero-dimensional fullerene and have emerged as promising nanomaterials for engineering next-generation biomedical devices. GNDs are environmentally friendly and demonstrate excellent biocompatibility compared to semiconductor quantum dots which usually include a toxic heavy metal (e.g., Cd) within their structure for attaining high-intensity fluorescence [1,2]. The band gap of the GNDs can be tuned via arranging the particle size and surface functionalities; thus, altering the integrity of π-electron and subsequently controlling the chemical structures [3]. Several groups have synthesized fluorescent GNDs from carbon, nitrogen and hydrogen precursors through a thermal pyrolysis method [4–6]. This technique is based on the carbonization of proper carbon sources into small molecules as the starting materials to chemically construct the desired GNDs. The pyrolysis method is a relatively fast and inexpensive technique which results in high production rate and yield for scale-up (industrial-scale synthesis of GNDs [2,7]. GNDs usually have an average particle size below 100 nm. Successful implementation of the GNDs has already been demonstrated for bio-imaging probes [8], optical detectors [9], light emitting diodes [10], visible-light-driven photocatalysts [11], supercapacitors [12], and Li-ion batteries [13]. However, functionalized GNDs have not been heavily explored for electronics since the influence of the functionalization on the thermal and electrical conductivity of the nanomaterials has remained unclear.

Thermal design of the nano-devices such as junctions and GNDs with the objective of enhancing the heat dissipation is of critical importance for developing graphene-based nano-electronics [14]. Controlling the thermal transport properties is essential for the design and fabrication of high-performance thermoelectric devices. Therefore, in this work, we report on chemically synthesized GNDs tailored for the heat dissipation applications. An efficient pyrolysis technique, based on thermal carbonization of citric acid and urea under IR irradiation at 200 °C, was developed to synthesize high-yield GNDs. The as-prepared

* Corresponding author at: Department of Chemical Engineering and Materials Science, Yuan Ze University, Taoyuan 32003, Taiwan.
E-mail address: cthsieh@saturn.yzu.edu.tw (C.-T. Hsieh).

https://doi.org/10.1016/j.tsf.2019.137704
Received 9 September 2019; Received in revised form 17 November 2019; Accepted 18 November 2019
Available online 18 November 2019
0040-6090/ © 2019 Elsevier B.V. All rights reserved.

GNDs were found to have a large amount of oxygen and nitrogen functionalities (e.g., C–OH, C==O, O–C==O, O==C–N and O==C–NH_2) at the edge and on basal plane of graphite-like powders. It is generally recognized that the band gap of oxidized graphene sheets increases with an increase in O/C atomic ratio since it shifts the band-structure from zero-gap to finite-gap semiconductor [15]. This observation implies that the transport of collective vibrations or phonons responsible for heat conduction in semiconductor and dielectric materials mainly originates from the presence of intrinsic defects, point defects, topological defects, edge termination, surface roughness, surface heterogeneity, and voids or cavities in the carbon layers [16,17]. Some previous experimental and modeling works have explored the variations in the thermal and electrical transport properties induced by the edge disorder and the crystallographic orientation of the graphene edges within the nano-sized graphene [18].

In this work, our major motivation was to explore the influence of various thermal treatment schemes on the thermal and electrical conductivity of GND-based polymeric layers. An IR-assisted pyrolysis was initially adopted to synthesize the functionalized GNDs; subsequently, a thermal reduction at 400 °C in the presence of helium was carried out to strip some oxygen functional groups from GND surface. Five types of GND-based thin films, mixed with water-based binder (i.e., polyvinylpyrrolidone (PVP) and polyvinyl alcohol (PVA)), were prepared. A series of experiments were conducted to assess the thermal conductivity (k) of the samples within the temperature range of 80–140 °C. The correlation between k and electrical conductivity (σ) on GND-based thin films was established as well. This work aims at the breakthrough of fast progress on thermal management of interfacial GND surfaces, providing a pioneering framework for evaluating the heat dissipation and thermal management within nano-engineered electronic devices.

2. Methods

2.1. IR-assisted synthesis of functionalized GNDs

An IR-assisted synthesis technique was adopted using a customized furnace equipped with six medium-wave IR filaments with the wavelength in the range of $1.4-3.2$ μm. The nominal power density of the IR filaments was 80 kW/m^2. The near-IR heaters were capable of delivering the thermal energy in the form of the electromagnetic radiation, i.e., with no need to any medium between the two bodies for the energy transfer. The carbon precursor, citric acid (15 g) and urea (5 g), were uniformly mixed. Subsequently, the solid mixture was placed into the IR furnace and heated to 200 °C with a heating rate of 20 °C/min. The IR heating process was stabilized at 200 °C in the air for 40 min. After cooling down to ambient temperature, the black powder was sieved through a stainless foil mesh (Type: 200 mesh), collecting GND samples. To inspect the effect of surface functionalities, GND powders were placed within the high-temperature furnace for conducting the treatment. The thermal treatment was carried out via heating the GND samples from the room temperature to 400 °C (with a ramping rate of 10 °C/min) and maintaining the temperature at 400 °C for 30 min under a steady-state helium flow. Throughout this paper, the GND samples were designated as GND1 for the samples with thermal treatment and GND2 for the ones without any treatment.

To evaluate the performance of as-prepared GNDs, a comparison has been made with another commonly used two-dimensional material (i.e. reduced graphene oxide (RGO)). The RGO sample was prepared using a modified Hummers' method [19], in which natural graphite powders (particle size: 5–10 μm) were chemically exfoliated via a strong oxidation agent. Upon chemical exfoliation, the resulting graphene oxide sheets were placed into a microwave reactor (maximal power: 900 W) and thermally reduced to RGO sheets in ethylene glycol at 90 °C for 30 min.

Five types of GND-containing polymeric thin films were prepared and subsequently coated onto Cu foils. First, the polymers, PVP (Alfa Aesar, purity: 99%) and PVA (Alfa Aesar, purity: 98%), were separately dispersed in distilled water (with an identical weight ratio of 1:1). Afterward, PVA solution (15 mL) was well mixed with PVP solution (30 mL), resulting in the PVA-PVP mixture. The as-prepared GND powders were then poured into the mixture and the GND slurry was stirred at ambient temperature using a magnetic bar for 1 h. Five GND weight loadings, 17, 29, 38, 44, and 50 wt%, were prepared to elaborate the influence of GND loading on the thermal and electrical conductivity of the GND-based heat sinks. Commercially available metallic foil, Cu, with a nominal thicknesses of 15 μm was employed as the heat sink substrate. A slurry-coating technique was adopted to prepare the carbon coating onto the metallic foil for thermal conductivity measurements. The GND slurries were pasted on the metallic foil substrates with a doctor blade (slot thickness: 200 μm), followed by an induced solvent (i.e., distilled water) evaporation with a blow dryer. Afterward, as-prepared GND layers were dehydrated at 105 °C in an oven overnight. Finally, GND sheets were cut into a sample size of 50 × 50 mm for measuring the thermal (k) as well as the electrical (σ) conductivities. The thickness of as-resultant GND layers was approximately 15–20 μm. A spray coating technique was also adopted to disperse the GND layers onto filter paper and cotton cloth. Based on the recipe detailed earlier, a single sprinkler was capable of spraying GND slurry onto cellulose filter paper (Whatman, diameter: 45 mm; thickness: 180 μm; pore size: 11 μm) and cotton cloth. Fresh cotton cloth substrate was made of fibers having a diameter of approximately $10-12$ μm. The thickness of the GND coating layers on both substrates (i.e., filter paper and cotton cloth) ranged from 100 to 200 nm.

2.2. Materials characterization of GND samples

Field-emission scanning electron microscope (FE-SEM) images were taken using a JEOL JSM-6701F electron microscope at an accelerating voltage of 10 kV. An X-ray diffraction (XRD; Shimadzu Labx XRD-6000) spectroscope, equipped with Cu-Kα radiation emitter (1.5405 Å), was employed to characterize the crystalline structures of the carbon materials. The XRD scans were performed at 2°/min from 10° to 80°. The maximal output of X-ray generator was 3 kV and the dimension of the XRD equipment was W900 × D700 × H1600. Raman spectra of carbon samples were recorded using a Raman spectrometer (Renishaw 2000 Raman microscope) with an excitation wavelength of 532 nm. An inductively-coupled plasma optical emission spectroscopy/mass spectrometry (ICP-OES/MS) was used to characterize the chemical compositions of GND samples. Fourier transform infrared (FT-IR) spectra of GND powders were acquired using Nicolet 380 spectrometer.

2.3. Electrical and thermal characterization of GND thin films

Prior to thermal and electrical conductivity measurements, all GND-coated Cu foils were dried at 110 °C in a vacuum oven for 12 h. A thin-film probing system (KeithLink Technology Co., Ltd.) was employed to measure the σ values of as-prepared GND thin films. The probe diameter and the probe spacing distance were approximately 100 μm and 1 μm, respectively. The σ value was determined through averaging five sample measurements recorded at different locations of the films.

An in-house test platform was designed and fabricated to assess the thermal conductivity of the GND-coated thin films. The test platform has been employed to measure thermal conductivities of other carbon-based thin films such as carbon nanotubes/graphene [21] and graphite nanosphere/graphene composite films [22]. The effective k value can be approximated using the Fourier's law [22]:

$$Q/A = k\Delta T/\Delta x \quad (1)$$

where Q is the magnitude of heat transfer through the thin films, A is the area normal to heat transfer direction, ΔT is the temperature difference over the thickness of the thin films (Δx), i.e., $\Delta T/\Delta x$: temperature gradient. High-purity Cu (i.e., 99.95%) and Al foils (i.e., 99.9%)

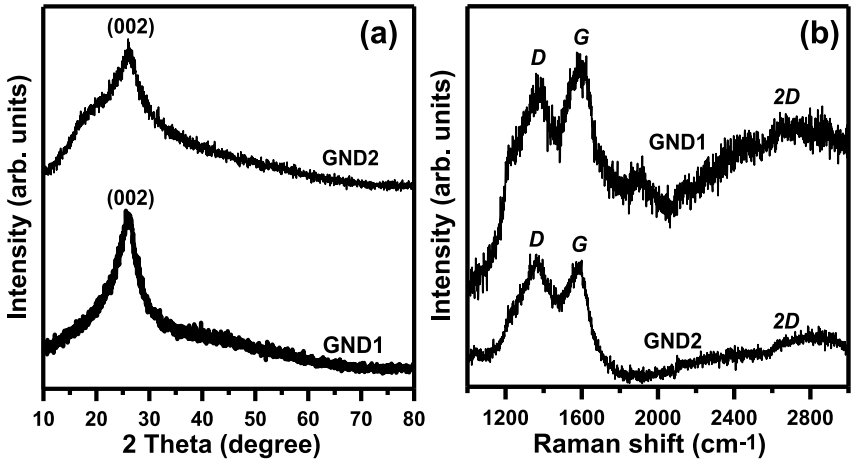

Fig. 1. Typical (a) XRD patterns and (b) Raman spectra of different GND samples.

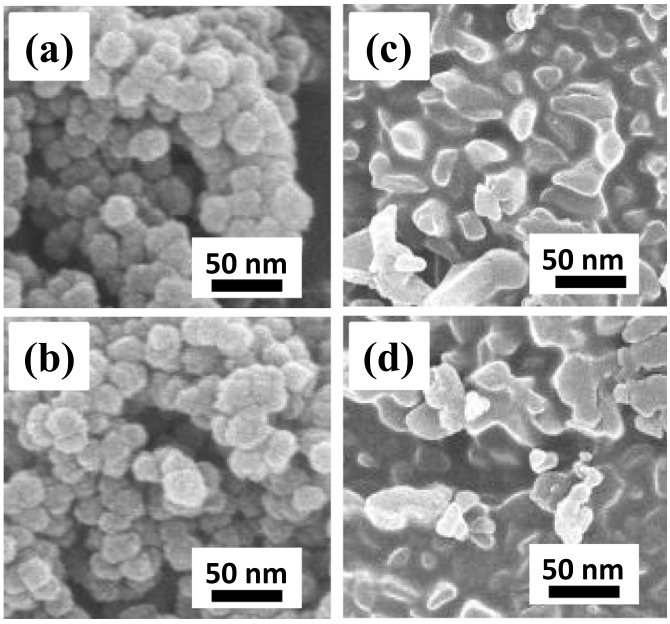

Fig. 2. FE-SEM images of (a) GND1 and (b) GND2 nanopowders. Top-view micrographs of (c) GND1 and (d) GND2 composite thin films.

were used as the reference material for calibrating the setup. The calibration temperatures ranged from 80 to 140 °C, to simulate the temperature range commonly observed within the chips used in consumer electronics. All the GND-coated thin films were insulated with heat-preservation cotton to avoid any heat dissipation. The temperature sampling was monitored and recorded using an array of five thermal-couples (*K*-type, accuracy: 0.1 °C) where one was used for the heater, three for the heat sink, and last one for the ambient temperature. The *k* values were determined via comparing the temperature drops across the thin films and subsequently using Eq. (1). Herein, the conductivity for each sample was evaluated based on the averaging over the data recorded at different locations of the thin films.

3. Results and discussion

Typical XRD patterns of as-received GND samples are shown in Fig. 1(a). As depicted in Fig. 1(a), the internal structure of both samples is highly crystalline due to the presence of $d_{(002)}$ peak. The $d_{(002)}$ peaks of GND1 and GND2 samples take place at 26.4 and 25.4°, respectively. Using Bragg's Law, the $d_{(002)}$ values are calculated to be 0.337 and 0.350 nm for GND1 and GND2 samples, respectively. It is essential to note that the interlayer distance of highly oriented graphite carbon is approximately 0.335 nm [23], very close to that of GND1 sample in this case. This result reveals that GND1 sample possesses a graphitized crystal through the IR-assisted pyrolysis of critic acid and urea, followed by thermal treatment at 400 °C.

Typical Raman spectra of both samples are provided in Fig. 1(b). As shown in Fig. 1(b), the Raman spectra contain three main peaks: *D* band (~1380 cm^{-1}), *G* band (~1600 cm^{-1}), and 2*D* band (~2700 cm^{-1}). The *G* band mainly originates from a single crystallite of graphite, whereas the *D* band is frequently ascribed to amorphous carbon or deformation vibrations of a hexagonal carbon ring [24,25]. The intensity ratio of *D* to *G* bands usually serves as an important index to evaluating the graphite degree of carbon-based materials. The intensity ratios of GND1 and GND2 samples are 0.92 and 1.05, respectively. This result reveals that the crystalline degree of carbon samples has been significantly improved by thermal treatment, which is in good agreement with the XRD analysis. This enhanced crystallinity can be attributed to the fact that the thermal treatment is able to (i) strip oxygen and nitrogen functional groups, (ii) reform or heal some defects in curved graphene sheets, and (iii) terminate dangling bonds within crystal lattice plane. Interestingly, the 2*D* band at ~2700 cm^{-1} is viewed in the Raman spectra of both GND1 and GND2 samples. The position and shape of 2*D* peak are pivotal index to characterize the number of graphene layers. Accordingly, the number of graphene layers is approximately 10, according to the standard Raman spectra at 514 nm [26].

FE-SEM images of GND1 and GND2 samples are given in Fig. 2(a) and (b), respectively. These images clearly reflect that both GND1 and GND2 samples exhibit a spherical form with an average particle size of 20–30 nm. Accordingly, the thermal treatment has an insignificant effect on the particle size of GND samples since the size of the samples remain relatively unchanged after the treatment. The production yield of GND samples through the IR synthesis method can attain as high as ~40 wt% for GND1 and GND2 samples. This finding reveals that the IR-assisted synthesis method can be well-suited for the large-scale production of functionalized GND powders. As shown in Fig. 2(c) and (d), each nanoparticle tends to be glued together and thus form a continuous layer on Cu foil upon coating the GND-based PVA-PVP polymeric layers. For comparison, the micro-structural morphology of RGO sheets as well as the thin films has been provided in Fig. 3. The surface of the aggregated sheets is fairly flexible, and a layered and loose structure can be observed at the edge of the agglomerates. The random arrangement of the nanosheets imparts the formation of a porous structure that contains micropores and mesopores.

An ICP-OES/MS analysis was employed to uncover the chemical compositions of as-prepared GND samples. According to the ICP-OES/MS measurement, the N/C and O/C atomic ratio for the GND1 sample is

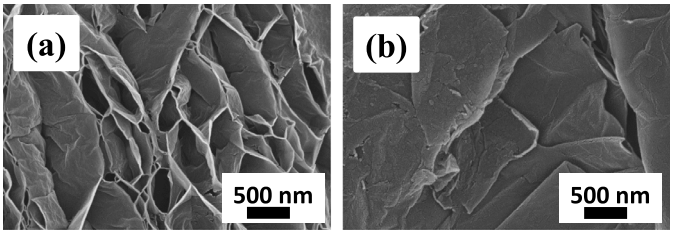

Fig. 3. FE-SEM images of (a) RGO sheets and (b) RGO composite thin film.

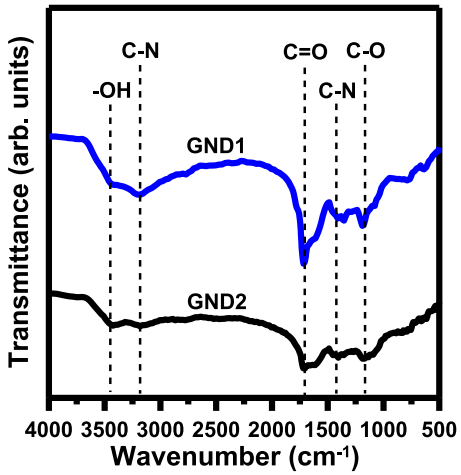

Fig. 4. FT-IR spectra of different GND samples.

14.1 and 17.7 at%, respectively, where for the GND2 sample the atomic ratios are noticeably higher (22.8 at% and 35.1 at% for the N/C and O/C, respectively). It is important to note that the RGO sample possesses a fairly high O/C ratio although the O/C ratio was reduced from 46.1 at% to 22.3 at% with the aid of microwave-assisted reduction in ethylene glycol. This result reveals that an oxidized surface coverage appears on RGO sample and numerous surface functional groups still occupy at edge or on basal plane of RGO sheets.

To inspect nitrogen and oxygen functionalities, FT-IR spectra, as illustrated in Fig. 4, were obtained to confirm the presence of surface functional groups on both samples. For both samples, one strong peak in the range of 1150–1300 cm^{-1} can be assigned to the contributions from the C–O stretch of –COOH, revealing the presence of hydroxyl and carboxyl functional groups on both samples [27–29]. Two apparent peaks occurring at ca. 1400 and 1706 cm^{-1} is ascribed to the existence of C–N and C=O functional groups, respectively [30]. One weak band at ca. 3400 cm^{-1} is mainly attributed to the physically adsorbed water molecules on the surface of both samples. It is worth noting that the relative transmittance intensity of GND1 sample is apparently reduced after the thermal treatment. This result is consistent with the analysis of XRD, Raman, and ICP-OES/MS. Therefore, it can be deduced that the IR-assisted synthesis method followed by a thermal treatment offers an effective pathway to produce highly crystalline GND samples. The post thermal process can be considered as an efficient way to finely tune the surface heterogeneity and crystallinity of graphite-like nanoparticles, e.g., surface amidation and oxidation levels.

Photographs of GND1 and GND2 polymeric coating layers onto copper foils and cellulose filter papers under UV irradiation (360 nm) are illustrated in Fig. 5(a)–(c). Herein, the weight loading of GND in the slurry was set at 50 wt%. As illustrated in Fig. 5, the GND-based coating layers emit blue and green lights at 360 nm. Interestingly, the GNDs still exhibit a tunable fluorescent emission from green to blue color (i.e., blue shift) after thermal treatment at 400 °C. This spectral change is significantly influenced by the amidation and oxidation extent on GND surface. It is well known that N- and O-doping or decorating modify the

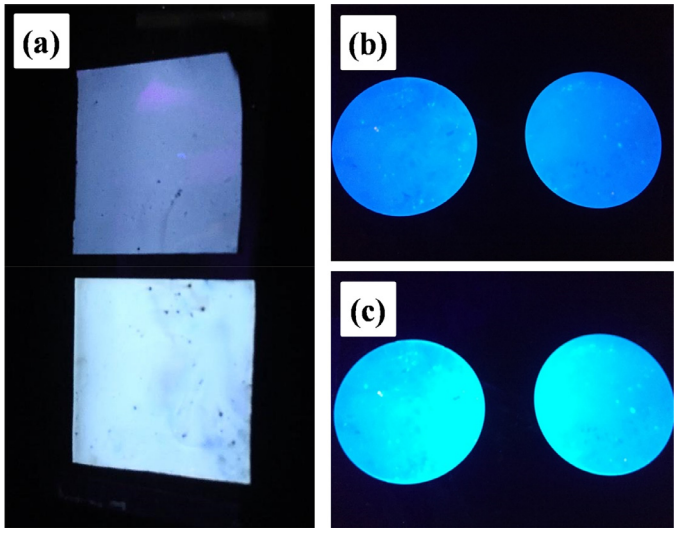

Fig. 5. (a) Top-view photographs of GND thin films on Cu foils (top: GND1 and bottom: GND2). Photographs of (b) GND1 and (c) GND2 coatings onto filter papers.

electronic density of semiconductor materials and thus alter the optical properties [31]. Theoretically, N-doped graphene, i.e., electron-rich nitrogen, enables an in-plane substitution of N atoms to graphene as *n*-type semiconductor [31,32]. In this case, the thermal treatment is capable of removing a significant percentage of the hydroxyl and carboxyl group, serving as non-radiative electron-hole recombination center [33]. Thus, the GND samples exhibit an adjustable fluorescence emission due to the influence of thermal treatment.

Fig. 6(a) and (b) show the k values as a function of temperature for different configurations of the thin films on Cu substrates (50 and 17 wt % carbon content). As illustrated in Fig. 6, the k values demonstrate a decreasing function of temperature due to an increase in phonon population at higher energy states which subsequently induces an increase in phonon scattering at high temperatures [16]. Notably, the decreasing function is incompatible with the Umklapp phonon-phonon scattering that suggests $1/T$ temperature-dependence characteristics [34]. The GND1 thin film offers the highest k value among all the samples for the temperature range between 80 and 140 °C. At 80 °C, the k value has an order as GND1 (855 W/m K) > GND2 (770 W/m K) > RGO (727 W/m K) at 50 wt% carbon content. The same sequence also holds for the k value at 17 wt% carbon content. It is generally recognized that the thermal conduction in carbon materials is mainly dominated by phonon-boundary scattering, related to lattice vibration and phonon mean free path in basal planes [35]. The presence of oxygen functionalities would impart an increase in band gap of graphene sheets [15], thus promoting the phonon scattering. Additionally, hydrogenation is one of the key factors in determining surface heterogeneity of carbon-based heat sinks. The deterioration of thermal conductivity possibly originates from the sp^2-to-sp^3 bonding transition upon hydrogenation [36], tuning the thermal conductivity of graphene sheets. This phonon scattering is unfavorable for thermal conduction in carbon materials due to a short phonon mean free path, causing a substantial thermal junction. Due to the low oxidation levels, well-dispersed GND1 powders form a three-dimensional conductive network, leading to higher thermal conductivity. As for both GND2 and RGO samples, the thermal carriers (e.g., phonon) on both films are more restricted at highly oxidized surface coverage (i.e., GND2 and RGO thin films). Moreover, randomly-stacked RGO sheets tend to be isolated in the PVA-PVP polymeric films without a homogeneous dispersion. Since through-plane k value is significantly lower than in-plane thermal conductivity on two-dimensional graphene sheets, it is more difficult to build up an integrated skeleton for thermal diffusivity in RGO thin film. Thus, the

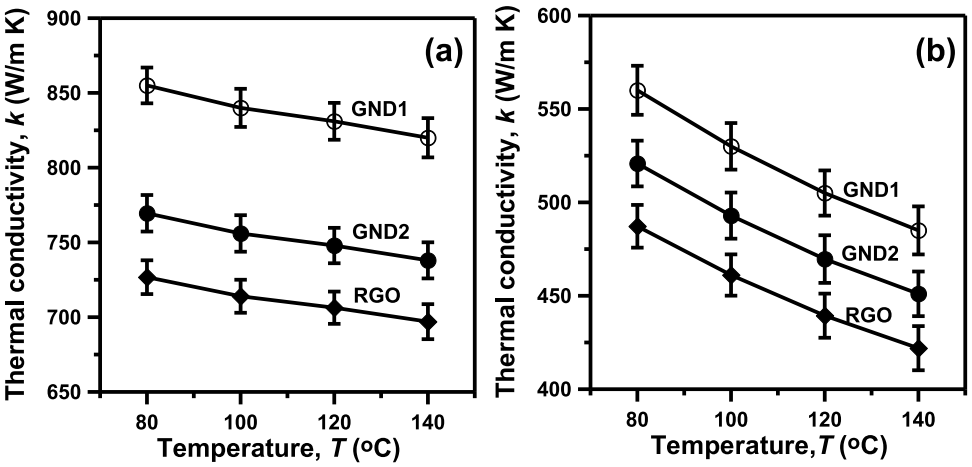

Fig. 6. Thermal conductivity as a function of operating temperature at (a) 50 wt% and (b) 17 wt% carbon content.

phonon mean free paths on both films are dramatically reduced, resulting in highly resistive thermal junctions. With increasing the weight loading, GND1 nanopowders further enhance the heat dissipation, thus favoring the thermal management in ultra-small scales.

To further analyze this trend, the variations in the thermal conductivity of the composite films was explored at 80 and 140 °C, as shown in Fig. 7(a) and (b), respectively. As depicted in Fig. 7, there is an inflection point between 17 and 38 wt% carbon content, i.e., at 29 wt%. After that, a linear relationship between the thermal conductivity and the carbon content in the heat sink can be obtained. Data from Fig. 7(a), the correlation factors (r^2) are 0.988, 0.988, and 0.989 for the linear plots of GND1, GND2, and RGO samples, respectively. The r^2 values range from 0.932 to 0.997, resulted from the linear plots of Fig. 7(b). It is commonly accepted that pure PVA polymeric films demonstrate poor thermal conductivity; this trend was further confirmed with the measurements conducted in this work (i.e. 0.31 W/m K) [37]. In contrast, graphene sheets, consist of one or few layers of atoms arranged in a honeycomb lattice, has theoretical k value of 4840–5300 W/m K for a single-layer graphene [38,39]. Therefore, the carbon content plays a crucial role facilitating the k value of the composite films. Maintaining the carbon content at 29 wt% results in a significant enhancement of the thermal conductivity for the samples considered in this work. This is presumably due to the formation of a continuous conductive network of carbon nanodots at high carbon content which ultimately boats the thermal conductivity within the composite films. The percolation theory can be used to explain the variation of thermal conductivity with the GND solid content in the composite films [36]. At the transition point (i.e., 29 wt% GND), the thermal pathway was created due to the formation of continuous conducting network of C nanodots. Thus, the three-dimensional network percolation developed by GNDs induces better thermal conduction and less photon scattering. For clarification, one schematic diagram illustrating thermal pathways in different composite films, including pristine PVP-PVA, low-density GNDs mixed with PVP-PVA (e.g., GND2 coating at 17 wt%), high-density and highly oxidized GNDs mixed with PVP-PVA (e.g., GND2 coating at 50 wt%), and high-density and thermally-treated GND mixed with PVP-PVA (e.g., GND1 coating at 50 wt %) composite films, has been schemed, as shown in Fig. 8. This reveals that the high-density and thermally-treated GNQs mixed with PVP-PVA composite film creates a well-developed conductive network for thermal conduction, inducing higher k value.

Pioneering studies have reported on the strong correlation between the electrical conductivity (i.e., free electrons in materials) and the thermal conductivity (i.e. lattice vibration and phonon transport) [40,41]. The relationship between thermal resistivity and electrical resistivity at ambient temperature for graphitized carbons has been investigated by Mason and Knibbs in 1962 [42]. To explore the interaction between the thermal and electrical conductivities, the electrical resistivity of GND1, GND2, and RGO thin films was measured as illustrated in Fig. 9(a). According to Fig. 9(b), the k values demonstrate an increasing trend with the increased in σ value for the temperature range of 80–140 °C. The r^2 values for the linear plots fall into the region of 0.958–0.997. This observation confirms that the presence of oxygen functionalities suppresses both thermal and electronic transport on

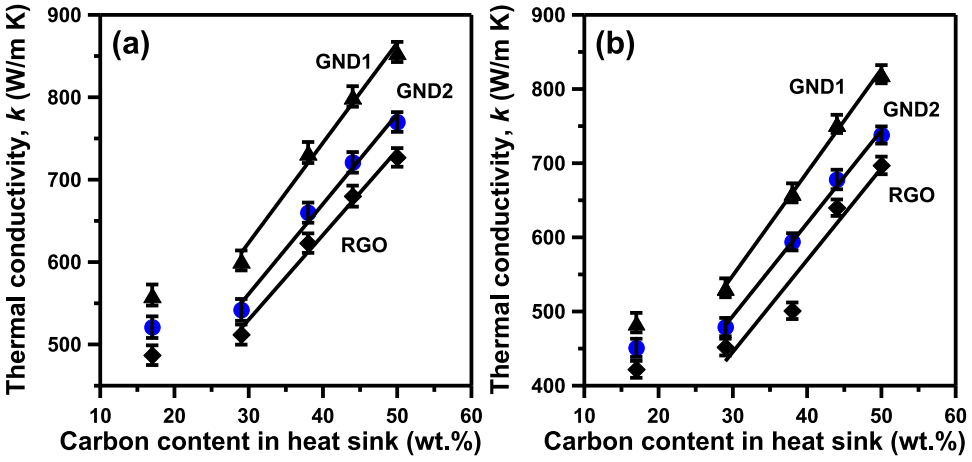

Fig. 7. Thermal conductivity as a function of carbon content in composite thin films at (a) 140 °C and (b) 80 °C.

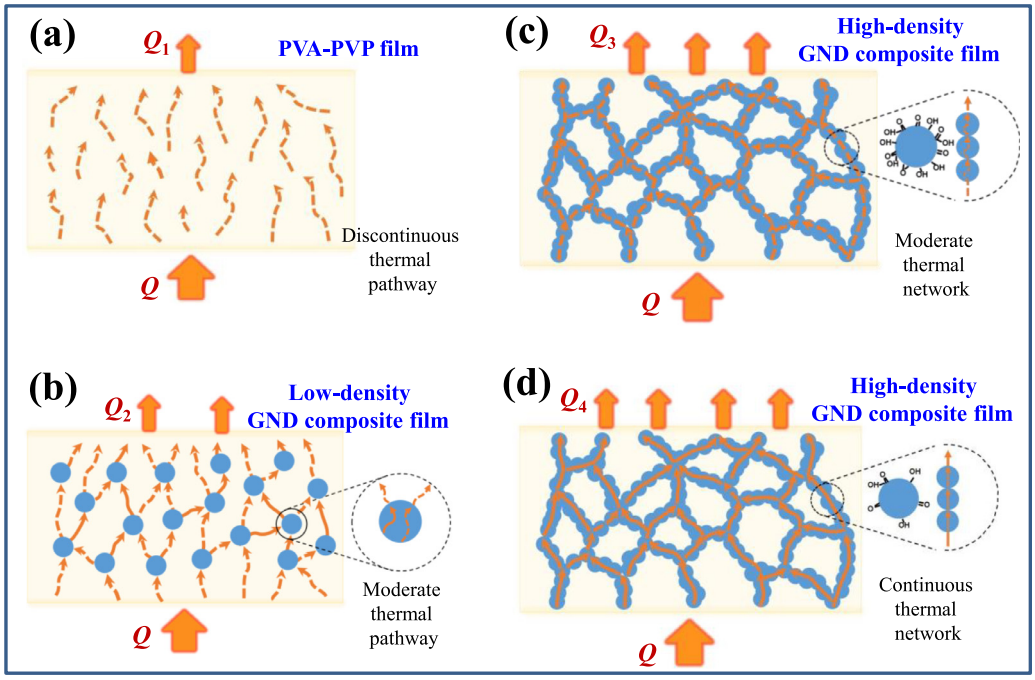

Fig. 8. Schematic diagram illustrating thermal pathways in different composite films: (a) pristine PVP-PVA, (b) low-density GNDs mixed with PVP-PVA, (c) high-density and highly oxidized GNDs mixed with PVP-PVA, and (d) high-density and thermally-treated GND mixed with PVP-PVA composite films. Herein Q represents heat transfer rate from heat source, and Q_1, Q_2, Q_3, and Q_4 represent heat transfer rate out of different heat sinks.

GND thin films. To inspect the ratio of thermal to electronic conduction in the composite films, the Lorenz numbers (L) were calculated, based on the Wiedemann-Franz Law ($k/\sigma = LT$) that states the ratio between thermal conduction and electronic conduction in a material is proportional to temperature (T) [43]. Data from Fig. 7, the L values at 80 °C has an order as 8.58×10^{-4} W Ω/K^2 (RGO) > 4.74×10^{-4} W Ω/K^2 (GND2) > 3.64×10^{-4} W Ω/K^2 (GND1) at 50 wt%. As for 17 wt%, the L values show an obvious decease but the same sequence is acquired: 5.75×10^{-4} W Ω/K^2 (RGO) > 3.21×10^{-4} W Ω/K^2 (GND2) > 2.38×10^{-4} W Ω/K^2 (GND1). This reveals two crucial messages: (i) the introduction of GNDs is favorable for thermal conduction, and (ii) the GND with low oxidation level is beneficial for electronic conduction at the identical carbon content in the composite films.

To explore the feasibility of this approach for heat sink applications, a heat dissipation measurement was conducted to analyze the variations in the surface temperature of GND1-coated cotton cloth samples overtime. Initially, a hot plate was heated to about 95 °C and maintained at this temperature to achieve steady state conditions. The GND1-coated cloth (area: 15 × 15 cm^2) was subsequently coated on the hot plate. Finally, the heating source of the plate was turned off and a thermal imaging instrument was used to record the surface temperature distribution on the treated cloth. The thermal imaging patterns for the clothes with and without GND1 coating layer have been illustrated in Fig. 10(a) and (b), respectively. Obviously, the surface temperature of original cloth tends to slowly decrease from 93.9 to 35.6 °C within 16 min, whereas the temperature of GND1-coated cloth demonstrates an increased cooling rate (from 94.7 to 27.6 °C within 16 min). The variation of surface temperature with cooling time is depicted in Fig. 10(c). We observe that temperature difference between original and treated cloth gradually becomes evident, indicating that GND1 coating displays an enhanced thermal dissipation. For comparison, the cooling rates are calculated to be 3.6 and 4.2 °C/min for untreated and GND1-coated cloth, respectively. This reveals that the heat thermal dissipation of the cloth is enhanced by 16.7%. This enhancement can be ascribed to the creation of thermal conduction network, where cotton fabrics can be regarded a skeleton and the GND-1 films are strictly attached to the fabrics with the aid of PVP-PVA binder. Based on the percolation theory, the hierarchical GND1-coated cotton cloth creates a thermally conductive network that offers more surface contact and point-by-point connection, thus, allowing more efficient heat transport

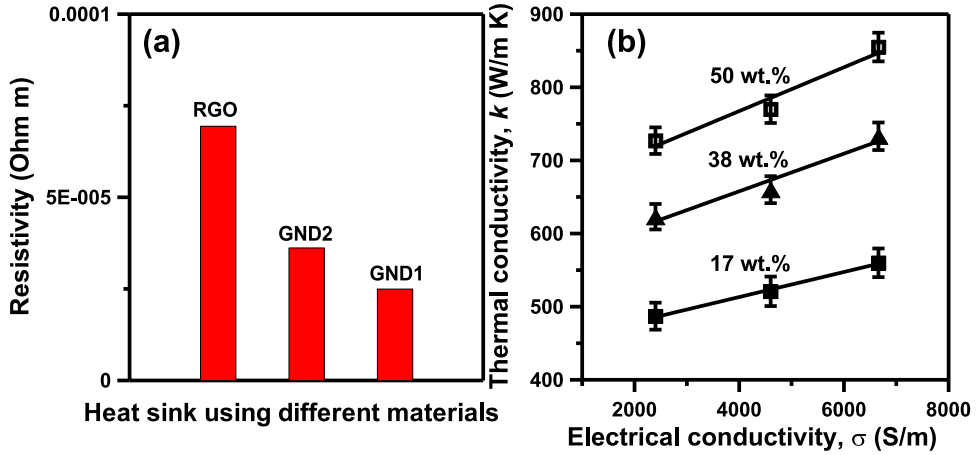

Fig. 9. (a) Electrical resistivity varied with type of composite thin films using different materials. (b) Thermal conductivity at 140 °C as a function of electrical conductivity.

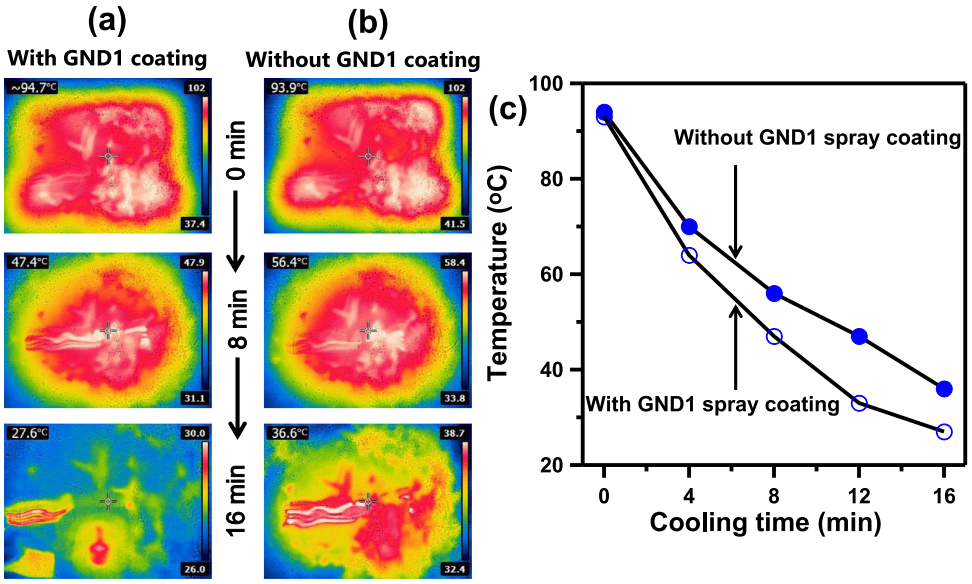

Fig. 10. Thermal imaging pictures of cotton cloth (a) with and (b) without GND coating after 0, 8, and 16 min. (b) Surface temperature as a function of cooling time.

[20]. Accordingly, the design of hierarchical GND1 thin film is promising for enhanced thermal management of electronic and photonic applications thanks to efficient fabrication technique, tunable fluorescence emission, and high thermal as well as electrical conductivity.

4. Conclusions

Herein we summarize the efforts to synthesize functionalized GNDs and to prepare GND-based composite films using PVA-PVP polymeric binder for devices requiring enhanced thermal and electrical conductivities within their nano-structures. This study demonstrated that the IR-assisted pyrolysis of citric acid and urea is capable of synthesizing crystalline GNDs at 200 °C. Thermal treatment was the pivotal factor affecting surface amidation/oxidation extent on GND surface and subsequently inducing tunable fluorescence. The GND thin films were found to illuminate a tunable fluorescence emission (i.e., from green to blue light) after thermal treatment of GNDs at 400 °C in helium atmosphere. The thermal conductivity of GND coated samples reached as high as 855 W/m K at 50 wt% carbon content in the composite thin films. The improved thermal conductivity mainly originated from the low oxidation level on GNDs, thus reducing the possibility of photon scattering. With increasing weight loading, GNDs can serve as scaffold creating a stereo conductive path for thermal dissipation. An empirical linear correlation was also established between the thermal and electrical conductivities. Therefore, the design of GND thin film provides a promising pathway towards nano-engineering devices with tunable fluorescence emission as well as improved thermal/electrical conductivities.

Declaration of Competing Interest

The authors declare that they have no known competing financial interests or personal relationships that could have appeared to influence the work reported in this paper.

Acknowledgment

Financial support from the Ministry of Science and Technology of Taiwan (MOST 108-2221-E-155-036-MY3) is greatly acknowledged.

References

[1] X. Zhai, P. Zhang, C. Liu, T. Bai, W. Li, L. Dai, W. Liu, Highly luminescent carbon nanodots by microwave-assisted pyrolysis, Chem. Commun. 48 (2012) 7955–7957.
[2] S.K. Bhunia, A. Saha, A.R. Maity, S.C. Ray, N.R. Jana, Carbon nanoparticle-based fluorescent bioimaging probes, Sci. Rep.-UK 3 (2013) 1473.
[3] L. Lin, M. Rong, F. Luo, D. Chen, Y. Wang, X. Chen, Luminescent graphene quantum dots as new fluorescent materials for environmental and biological applications trend, Anal. Chem. 54 (2014) 83–102.
[4] Y. Wang, A. Hu, Carbon quantum dots: synthesis, properties and applications, J. Mater. Chem. C 2 (2015) 6921–6939.
[5] S. Bak, D. Kim, H. Lee, Graphene quantum dots and their possible energy applications: a review, Curr. Appl. Phys. 16 (2016) 1192–1201.
[6] D. Qu, M. Zheng, J. Li, Z. Xie, Z. Sun, Tailoring color emissions from N-doped graphene quantum dots for bioimaging applications, Light Sci. Appl. 4 (2015) 1–8 e364.
[7] Y. Xu, M. Wu, Y. Liu, X. Feng, X. Yin, X. He, Y. Zhang, Nitrogen-doped carbon dots: a facile and general preparation method, photoluminescence investigation, and imaging applications, Chem. Eur. J. 19 (2013) 2276–2283.
[8] Q. Li, T.Y. Ohulchanskyy, R. Liu, K. Koynov, D. Wu, A. Best, R. Kumar, A. Bonoiu, P.N. Prasad, Photoluminescent carbon dots as biocompatible nanoprobes for targeting cancer cells in vitro, J. Phys. Chem. C 114 (2010) 12062–12068.
[9] A. Zhu, Q. Qu, X. Shao, B. Kong, Y. Tian, Carbon-dot-based dual-emission nanohybrid produces a ratiometric fluorescent sensor for in vivo imaging of cellular copper ions, Angew. Chem. Int. Ed. 51 (2012) 7185–7189.
[10] X. Guo, C. Wang, Z. Yu, L. Chen, S. Chen, Facile access to versatile fluorescent carbon dots toward light-emitting diodes, Chem. Commun. 48 (2012) 2692–2694.
[11] B. Y.Yu, S. Kwak, Carbon quantum dots embedded with mesoporous hematite nanospheres as efficient visible light-active photocatalysts, J. Mater. Chem. 22 (2012) 8345–8353.
[12] W.W. Liu, Y.Q. Feng, X.B. Yan, J.T. Chen, Q.J. Xue, Superior micro-supercapacitors based on graphene quantum dots, Adv. Funct. Mater. 23 (2013) 4111–4122.
[13] D. Chao, C. Zhu, X. Xia, J. Liu, X. Zhang, J. Wang, P. Liang, J. Lin, H. Zhang, Z.X. Shen, H.J. Fan, Graphene quantum dots coated VO_2 arrays for highly durable electrodes for Li and Na ion batteries, Nano Lett. 15 (2014) 565–573.
[14] Y. Xu, X. Chen, J.S. Wang, B.L. Gu, W. Duan, Thermal transport in graphene junctions and quantum dots, Phys. Rev. B 81 (2010) 1–7 195425.
[15] J. Ito, J. Nakamura, A. Natori, Semiconducting nature of the oxygen-adsorbed graphene sheet, J. Appl. Phys. 103 (2008) 1–5 113712.
[16] J. Haskins, A. Kınacı, C. Sevik, H. Sevinçli, G. Cuniberti, T. Çağın, Control of thermal and electronic transport in defect-engineered graphene nanoribbons, ACS Nano 5 (2011) 3779–3787.
[17] Y. Hong, J. Zhang, X. Huang, X.C. Zeng, Thermal conductivity of a two-dimensional phosphorene sheet: a comparative study with graphene, Nanoscale 7 (2015) 18716–18724.
[18] K.Y. Ritter, J.W. Lyding, The influence of edge structure on the electronic properties of graphene quantum dots and nanoribbons, Nat. Mater. 8 (2009) 235–242.
[19] W.S. Hummers Jr, R.E. Offeman, Preparation of graphitic oxide, J. Am. Chem. Soc. 80 (1958) 1339-1339.
[20] C.-T. Hsieh, C.-E. Lee, Y.-F. Chen, J.-K. Chang, H. Teng, Thermal conductivity from hierarchical heat sinks using carbon nanotubes and graphene nanosheets, Nanoscale 7 (2015) 18663–18670.
[21] C.-T. Hsieh, Y.-F. Chen, C.-E. Lee, Y.-M. Chiang, H. Teng, Thermal transport in stereo carbon framework using graphite nanospheres and graphene nanosheets, Carbon N. Y. 106 (2016) 132–141.

[22] S. Zhou, J. Xu, Q.H. Yang, S. Chiang, B. Li, H. Du, C. Xu, F. Kang, Experiments and modeling of thermal conductivity of flake graphite/polymer composites affected by adding carbon-based nano-fillers, Carbon N. Y. 57 (2013) 452–459.
[23] Q.M. Gong, Z. Li, Y. Wang, B. Wu, Z. Zhang, J. Liang, The effect of high-temperature annealing on the structure and electrical properties of well-aligned carbon nanotubes, Mater. Res. Bull. 42 (2007) 474–481.
[24] K. Kim, K. Kim, W.S. Jung, S.Y. Bae, J. Park, J. Choi, J. Choo, Investigation on the temperature-dependent growth rate of carbon nanotubes using chemical vapor deposition of ferrocene and acetylene, Chem. Phys. Lett. 401 (2005) 459–464.
[25] L. Ni, K. Kuroda, L. Zhou, T. Kizuka, K. Ohta, K. Matsuishi, J. Nakamura, Kinetic study of carbon nanotube synthesis over Mo/Co/MgO catalysts, Carbon N. Y. 44 (2006) 2265–2272.
[26] A.C. Ferrari, J.C. Meyer, V. Scardaci, C. Casiraghi, M. Lazzeri, F. Mauri, S. Piscanec, D. Jiang, K.S. Novoselov, S. Roth, A.K. Geim, Raman spectrum of graphene and graphene layers, Chem. Phys. Lett. 97 (2006) 1–4 187401.
[27] P.A. Hu Russo, G. Compagnini, W.W. Duley, N.Y. Zhou, Femtosecond laser ablation of highly oriented pyrolytic graphite: a green route for large-scale production of porous graphene and graphene quantum dots, Nanoscale 6 (2014) 2381–2389.
[28] B.P. Vinayan, Z. Zhaokarger, T. Diemant, V.S. Chakravadhanula, N.I. Schwarzburger, M.A. Cambaz, R.J. Behm, C. Kübel, M. Fichtner, Performance study of magnesium–sulfur battery using a graphene based sulfur composite cathode electrode and a non-nucleophilic Mg electrolyte, Nanoscale 8 (2015) 3296–3306.
[29] Z. Yang, Z. Yao, G. Li, G. Fang, H. Nie, Z. Liu, X. Zhou, X.A. Chen, S. Huang, Sulfur-doped graphene as an efficient metal-free cathode catalyst for oxygen reduction, ACS Nano 6 (2012) 205–211.
[30] P.R. Kharangarh, S. Umapathy, G. Singh, Thermal effect of sulfur doping for luminescent graphene quantum dots, ECS J. Solid State Sci. Technol. 7 (2018) M29–M34.
[31] F. Wu, J.T. Lee, A. Magasinski, H. Kim, G. Yushin, Solution-based processing of graphene-Li_2S composite cathodes for lithium-Ion and lithium-sulfur batteries, Part. Part. Syst. Char. 31 (2014) 639–644.
[32] Z. Jin, J. Yao, C. Kittrell, J.M. Tour, Large-scale growth and characterizations of nitrogen-doped monolayer graphene sheets, ACS Nano 5 (2011) 4112–4117.
[33] Q. Mei, K. Zhang, G. Guan, B. Liu, S. Wang, Z. Zhang, Highly efficient photoluminescent graphene oxide with tunable surface properties, Chem. Commun. 46 (2010) 7319–7321.
[34] E. Pop, D. Mann, Q. Wang, K. Goodson, H. Dai, Thermal conductance of an individual single-wall carbon nanotube above room temperature, Nano Lett. 6 (2006) 96–100.
[35] S. Berber, Y.K. Kwon, D. Tomanek, Unusually high thermal conductivity of carbon nanotubes, Phys. Rev. Lett. 84 (2000) 4613–4616.
[36] Q.-X. Pei, Z.-D. Sha, Y.-W. Zhang, A theoretical analysis of the thermal conductivity of hydrogenated graphene, Carbon N. Y. 49 (2011) 4752–4759.
[37] X. Xie, D. Li, T.-H. Tsai, J. Liu, P.V. Braun, D.G. Cahill, Thermal conductivity, heat capacity, and elastic constants of water-soluble polymers and polymer blends, Macromolecules 49 (2016) 972–978.
[38] Z.F. Li, H. Zhang, Q. Liu, Y. Liu, L. Stanciu, J. Xie, Novel pyrolyzed polyaniline-grafted silicon nanoparticles encapsulated in graphene sheets as Li-Ion battery anodes, ACS Appl. Mater. Interfaces 6 (2014) 5996–6002.
[39] B. Xie, C. Yang, Z. Zhang, P. Zou, Z. Lin, G. Shi, Q. Yang, F. Kang, C.P. Wong, Shape-tailorable graphene-based ultra-high-rate supercapacitor for wearable electronics, ACS Nano 9 (2015) 5636–5645.
[40] M. Zhou, H. Bi, T. Lin, X. Lü, D. Wan, F. Huang, J. Lin, Heat transport enhancement of thermal energy storage material using graphene/ceramic composites, Carbon N. Y. 75 (2014) 314–321.
[41] P. Keblinski, S. Phillopt, S. Choi, J.A. Eastman, Mechanisms of heat flow in suspensions of nano-sized particles (nanofluids), Int. J. Heat Mass Transf. 45 (2002) 855–863.
[42] I.B. Mason, R.H. Kinbbs, The Thermal Conductivity of Artificial Graphite and its Relationship to Electrical Resistivity, United Kingdom Atomic Energy Authority, 1962, p. 3973. AERE-R.
[43] Z. Xu, Heat transport in low-dimensional materials: a review and perspective, Theor. Appl. Mech. Lett. 6 (2016) 113–121.